Journal of Magnetism and Magnetic Materials 467 (2018) 37–48

Contents lists available at ScienceDirect

Journal of Magnetism and Magnetic Materials

journal homepage: www.elsevier.com/locate/jmmm

Review Articles

Layer-by-layer assembled iron oxide based polymeric nanocomposites

Maria A.G. Soler

Universidade de Brasilia, Instituto de Fisica, 70910-900 Brasilia-DF, Brazil

ARTICLE INFO

Keywords:
Magnetic nanocomposites
Iron oxide nanoparticle
Polymers
Layer-by-layer assembly
Dipolar interactions
Ferrites

ABSTRACT

Hybrid nanocomposites are nowadays the focus of intensive scientific and industrial research motivated by expectations from fields as diverse as microelectronics and medicine. One of the challenges faced by these materials, before getting into applications, is the development of methodologies capable of processing them in the form of thin planar nanostructures. To achieve this, bottom-up manipulation, such as the layer-by-layer approach capable of growing nano-objects while controlling position and inter-particle distances, has made possible the construction of assemblies with properties tailored on the nanoscale level. This review will summarize the new initiatives taken in the area of colloidal iron oxide nanoparticles and their arrays in polymeric matrix employing the layer-by-layer technique related research. Aiming to understand fundamental issues such as the effect of nanocomposite morphology on the collective magnetic properties, experiments and simulations performed to assess both the nanocomposite's morphology and the corresponding magnetic signatures, will be discussed. Applications leading to future developments related with these nanostructures, as for instance chemical sensors and storage devices, will also be highlighted.

1. Introduction

The assembly of molecular and nano objects – to build multifunctional materials, provides exciting opportunities for technologies at the interfaces between chemistry, physics, biology and nanomedicine – has been attracting significant interest in recent years [1–4]. The nanoparticles which possess unique geometrical shapes and media responsive optical, electronic and magnetic properties, have been employed as inorganic counterparts in nanocomposite assemblies [5–8]. In addition, recent development of colloidal synthesis methods and bottom-up approaches, enabled the production of organized 2- and 3-D nanostructures from DNA, enzymes, proteins, peptides, polymers, metallic and iron oxide nanoparticles, magnetic nanoparticles, graphene, carbon nanotubes, quantum dots, etc [9–15]. For most applications, ultrathin layers are required for the devicés active layers [16–18]. Among bottom-up approaches, the layer-by-layer (LbL) assembly [19–20], consisting of sequential adsorption of different molecules and nano objects, has been successfully employed. In this technique, different components are transferred and held together at the surface of a solid support by different types of intermolecular forces. This approach allows the design of all-organic and organic-inorganic multilayers with molecular-level control over the composition, morphology, thickness, and architecture. The LbL nanocomposites can be engineered on the surface of any type of solid support, ranging from smooth to rough, in any shape such as flat slides, rods, beads and in any size, of solid support from macro to nanoscale. In addition, LbL approach ensures efficient scale-up, cost effectiveness, and automation facilities [21–23]. The assembled nanostructures not only combine attractive functionalities of each component but also show synergetic characteristics, enabling them for multiple applications such as coatings, capacitors electrodes, storage energy, chemical sensors, and drug delivery systems [24–26].

Regarding magnetic nanomaterials, the LbL technique can be employed to assemble several types of superparamagnetic iron oxide nanoparticles (IONP) with common polyelectrolytes, resulting in nanocomposites with a synergistic combination of properties from both components [27]. Polyelectrolytes are essential in these types of nanocomposites, since they not only hinder nanocrystal agglomeration but also provide the mechanical and chemical stability of the nanomaterial. In addition, some types of polyelectrolytes may present electrical conductivity or response to temperature gradients, which thus turn films smart materials [28]. As inorganic magnetic components, IONPs, with small size (3–20 nm), exhibit novel size- and shape-dependent magnetic, electric, chemical, optical and thermal properties in comparison to their bulk counterparts. They are usually elaborated as stable colloidal dispersions, also known as magnetic fluids (MF), nanofluids or ferrofluids [29–32]. In particular, IONPs exhibit superparamagnetism [33,34] biocompatibility, and surface functionalities, making them very attractive for fundamental studies and a variety of potential applications [35,36], such as biomolecular separation [37],

E-mail address: soler@unb.br.

https://doi.org/10.1016/j.jmmm.2018.07.035
Received 1 March 2018; Received in revised form 2 June 2018; Accepted 10 July 2018
Available online 18 July 2018

nanocatalysis [38], rotating seals and magnetorheological vibration dampers [39], magnetic recording media [40], SERS probe [41], insulating oil for improvement of transformer's cooling efficiency [42], sensors [17,25,43–44], and biomedical applications [45–48]. Interesting, under external magnetic field, colloidal suspensions of IONPs exhibit reversible physical properties. For instance, the thermal conductivity of colloidal magnetite suspensions can be increased by changing the linear aggregation length from nano- to micron scales [32]. Systematic studies about the effect of applied magnetic field on the tunability of the thermal conductivity and viscosity of colloidal IONPs has demonstrate that magnetically controllable colloidal IONPs can behave like a multifunctional "smart" material that can remove heat and also arrest vibrations acting as a damper, opening an opportunity for applications in microfluidic devices [32,49].

IONPs can also be encapsulated inside the oil droplet during the emulsification process, using an anionic surfactant of sodium dodecyl sulphate as a stabilizer. It allows to one produce oil-in-water (O/W) ferrofluid emulsions [50]. These magnetic responsive nanoemulsions have been employed as non-enzymatic approach for glucose [51], and urea detection [52]. In another approach, magnetic emulsion stabilized with poly(N-isopropylacrylamide) (PNIPAM) were employed to prepare thermally tunable grating [53]. The temperature responsive conformational changes of PNIPAM, at the O/W interface, enables the inter-particle periodicity control. These thermo-magnetic multi-stimuli nanoemulsions are promising candidates for applications in visual and calorimetric sensors, temperature tunable grating, photonic materials, optical devices, and drug delivery systems [53].

The LbL technique has also been successfully employed for the preparation of magnetic nanocomposites, incorporating nanosized magnetite, maghemite, and cobalt ferrite, with different polyelectrolytes, including conducting polymers [24,25,27,54–76]. The magnetic nanoparticles, provided as aqueous colloidal dispersions, behave as electrolyte species. Thus they can be assembled through electrostatic interactions with oppositely charged polyelectrolytes. The inter-particle distances within the multilayered film can be finely tuned by varying physicochemical conditions of deposition dispersions, as well as by the number of deposited layers [62,69,70,72], or by manipulating the nanocomposite architecture [57,68,74]. Therefore, the LbL approach creates a unique window of opportunity to investigate morphological effects on magnetic nanocomposite properties, and in particular superparamagnetic behavior in quasi-bidimensional (2D) or 3D structures.

Through the years, LbL IONP/polymer nanocomposites have been investigated through both experiments and simulation of IONP adsorption kinetic, NP oxidation, morphology, structure, optical, dielectric, electrochemical and magnetic properties [24,25,54–76]. Furthermore, LbL-IONP/polymer structures present potential applications beyond the superparamagnetic behavior. The existence of $Fe2^+$ and $Fe3^+$ ions makes the iron oxide nanoparticles very useful for a variety of electrochemical devices, including electrodes for supercapacitors [24,76] and chemical sensors [17,25].

In this review, we shall focus mainly on recent progress in LbL nanocomposites comprising IONPs and polymers. Details of LbL assembly, and physicochemical aspects of mono and multilayer formation, nanocomposite morphology, and magnetic properties, as well as emerging applications, will also be discussed.

2. LbL assembly of nanocomposites

The LbL approach consists of the sequential dipping of a solid functionalized substrate into colloidal suspensions or polymer solutions of different species producing mono or multilayered assemblies held together by a wide range of intermolecular forces, including ionic interaction, hydrogen bonding, complexation, biospecific recognition, hybridization, hydrophobic interaction, and covalent attachment [9,21]. Furthermore, the LbL technique is quite inexpensive since it does not require clean rooms or sophisticated glassware, and is conducted at room temperature. Despite its simplicity, LbL provides an unprecedented control of film thickness and internal structure.

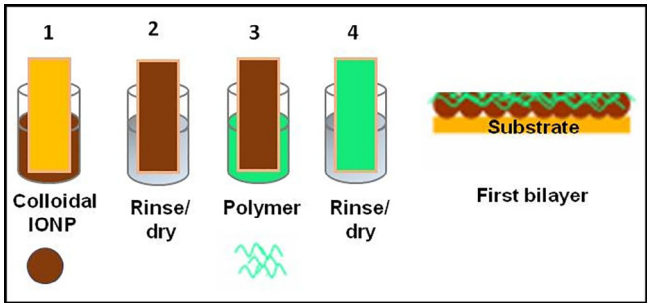

Scheme 1. Illustration of the LbL assembly of IONP/polymer nanocomposite and the first deposited bilayer.

Under electrostatic approach, the nanocomposite deposition starts with a functionalized substrate, comprising charged surface groups, being immersed into an oppositely-charged polyion solution, or NP dispersion. Because the charge balance between substrate surface and polyelectrolyte (or IONP) ionized groups, after a short period of time (order of few minutes) an ultrathin polyelectrolyte or NP monolayer is attached to the substrate and, the process proceeds and ends at its own. In fact, in the electrostatic LbL, the net charge of the substrate is overcompensated by the upcoming polyelectrolyte (or IONP) layer and the initial substrate charge is reversed [77]. When this condition is reached, the process ends and no more additional polyelectrolyte (or IONP) are adsorbed due to inherent electrostatic repulsions. Because of this character, the LbL is classified as a self-assembly method. During the deposition, the IONP/polymer bilayer is formed first, acting as the elementary repeating unit (see Scheme 1), the nanocomposite thickness can thus be increased by simply adding more IONP/polymer bilayers provided that anionic and cationic layers are adsorbed alternately.

Nanosized iron based cubic ferrites have been employed as inorganic counterparts in the LbL nanocomposite assembly. The chemical composition of cubic ferrites is MFe_2O_4, where M denotes a divalent transition-metal as Fe, Co, Ni, Mn, Cu, Zn, and Cd, which present ferrimagnetism magnetic ordering. Cubic iron oxide ferrites possess the spinel structure formed by a nearly close-packed face-centered cubic array of oxygen anions with interstices partly filled by metallic cations [29,78]. Maghemite (γ-Fe_2O_3) is an iron-deficient cubic ferrite [79], which is one of the most investigated iron oxides besides. In addition, magnetite has a half-metallic character with a large spin polarization at the Fermi level, presenting a high Curie temperature (850 K) and electrical resistivity of the same order of magnitude as a semiconductor. Hence it is a promising candidate for spintronic applications [80,81].

Bulk magnetic materials have a multi-domain structure, comprising regions of uniform magnetization surrounded by a domain wall (DW) structure. As the dimension of the magnetically-ordered material decreases towards the nanoscale, the typical domain-size and the DW-width decrease modifying its inner structure. Therefore, the orientation of the magnetization no longer splits into smaller domains, but instead maintains the magnetic structure of a single-domain. The magnetic behavior of a single-domain particle is described as a single "giant" spin, because of the atomic moments being aligned along the easy axis direction, which results in a big magnetic moment, called superparamagnetism. In the superparamagnetic regime, the orientation of the nanoparticle magnetic moment thermally fluctuates around the easy axis direction. The simplest picture describing the magnetic moment dynamics within the superparamagnetic particle is the one-dimensional symmetric double-well potential stemmed from the magnetocrystalline anisotropy. It lines up the magnetic moment in a particular crystallographic direction, as for instance the [111] direction in magnetite. However, thermal energy induces re-orientation of the magnetic

moment against the magnetrocrystalline energy barrier, resulting in fluctuation of the magnetic moment in a time scale of nanoseconds [29]. The typical relaxation time, ascribed to the average time that the magnetic moment takes for re-orientation with respect to the easy axis, is referred to as the Néel relaxation time [82].

IONP systems can be synthesized through chemical routes which allows a fine size control, size distribution, shape, crystallinity, and stability [83,84]. Further, the nanoparticle's surface can also be chemically engineered during their preparation via functionalization with different surface agents providing colloidal stability, making them as building blocks for LbL assembly, or as platform with anchoring sites to attach drugs and bio molecules [85–88].

The LbL assembly of IONP materials has been conducted via electrostatic interactions in conjunction with a large number of commercially available polyelectrolytes, including sodium sulfonated polystyrene (PSS), polyacrylic acid (PAA), polyallylamine hydrochloride (PAH), polydiallyldimethyl ammonium hydrochloride (PDAC), polyvinyl sulfonic acid (PVS), and polyethyleneimine. In addition, conjugated polymers in their doped state behave as polyelectrolytes as for instance, Polyaniline (PANI), poly(o-ethoxyaniline) (POEA), the polyelectrolyte complex poly(3,4-ethylenedioxy) thiophene:polystyrene sulfonic acid (PEDOT:PSS), and polypyrrole (PPy) [27].

The LbL assembly of colloidal dispersions [85] with oppositely charged polyelectrolytes is illustrated in Scheme 1. The LbL approach consists of the following steps: 1. immersion of the negatively-charged substrates for 3 min into positively charged IONPs dispersion (or polycation solution); 2. substrates are immersed in a rinsing aqueous solution (same pH of the previous immersion) for 20 s and blow-dried with nitrogen; 3. substrates are immersed for 3 min into polyanion solution (or IONPs); 4. immersion into the rinsing solution for 20 s (same pH of the previous immersion), and blow-dryed with nitrogen, resulting in the first deposited bilayer, as illustrated in Scheme 1. After repetition of the steps (1–4) n times, the resulting nanostructures will comprise n bilayers deposited on the substrate, and is usually represented by $(IONP/polymer)_n$ [27,67,69]. Indeed, the term 'bilayer' refers to a pair of cationic/anionic materials and not to a continuous layer of cationic material coated by a continuous layer of anionic material. These nanostructures are not stratified in definite layers as in molecular beam epitaxy or atomic layer deposited films [89,90]. In another approach, the assembly of a LbL multilayer film can be conducted by spraying the respective solutions/dispersions on the substrate. As for instance, Decher and coworkers compared the deposition of polyelectrolyte multilaryers by successive spraying polycation and polyanion solutions with the same assembled conditions using classic dipping [91]. The influence of assembly parameters such as spraying time, polyelectrolyte concentration, and film drying during multilayer deposition was investigated. It is found that the thickness of the multilayers increase linearly with the number of deposited cycles, as observed in the classic approach. The LbL assembly of films is very fast and leads to films with low surface roughness. Spray deposition allows regular multilayer growth even under conditions for which dipping fails to produce homogeneous films, such as extremely short contact times [91]. Afterwards, investigations of spray assisted LbL assembly of polyelectrolytes or colloidal particles have been conducted discussing the advances of this technique [92,93].

2.1. Build-Up of nanocomposites

The monitoring of the IONP/polymer LbL deposition onto glass slides can be carried out by UV–vis spectroscopy, in a simple and easy handling. Usually, UV–vis spectra of the starting materials, colloidal IONPs dispersions, and the polymer solutions, such as PSS and PANI are initially recorded [64]. Afterwards, the UV–vis spectra of nanocomposites are recorded at each assembled bilayer. Fig. 1 displays typical UV–vis spectra acquired during nanocomposite assembly (IONP/PSS)n for n = 2,4,6,8 and 10 bilayers. The inset exhibits the IONP absorbance

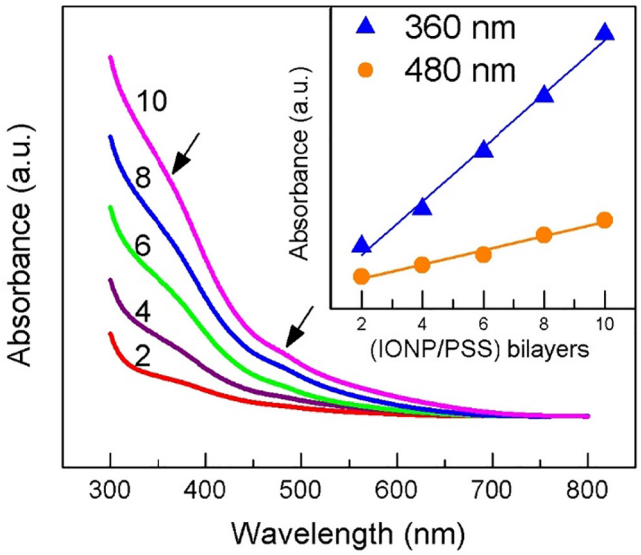

Fig. 1. UV–Vis spectra acquired after each deposited (IONP/PSS)n (n = 2, 4, 6, 8 and 10 bilayers). The inserted graphic exhibits the IONP absorbance at 360, and 480 nm, as a function of deposited bilayers [75].

at 360, and 480 nm, as a function of number of deposited bilayers. It is characteristic feature of magnetite because the ~~once~~ PSS does not show any absorption in the visible range. The amount of IONP increases almost linearly with number of the bilayers, indicating the growth of the film is in a stepwise manner [75]. Similar results are observed in other nanoparticle/polyelectrolyte systems where adsorption is driven by electrostatic attraction [67]. In another approach, Kim et al. investigated the LbL assembly of few bilayers of a structure comprising three layers of polymers (PSS/PPy) and two bilayers of PSS/IONP [58], through ellipsometry to monitor the nanocomposite deposition, estimating the thickness of each deposited bilayer.

The quartz crystal microbalance (QCM) technique can be employed to assess accurate kinetics and equilibrium parameters regarding the investigation of in situ adsorption of IONP [66]. When homogeneous and rigid ultrathin layers are adsorbed onto the surface of an oscillating crystal, the characteristic shift in frequency can be related to an increase in mass per unit area according to the Sauerbrey equation [94]. Regarding nanocomposite deposition, frequency shifts could be converted into mass of adsorbed species (IONP and/or polyelectrolyte), enabling mass detection up to the order of nanograms [66].

By using a QCM, coupled to a flow injection system, it is possible precisely monitor "in situ" the uptake of IONP on the surface of gold-coated quartz resonator inside the QCM cell. The investigation of the adsorption of $CoFe_2O_4$ nanoparticles onto the sodium 3-mercapto propanesulfonate, 3-MPS-functionalized gold-coated quartz resonator surface follows perfectly a first order kinetic process in a wide range (two orders of magnitude) of IONP concentrations [66]. These data were used to assess the equilibrium constant and the adsorption free energy [66]. Alternatively, the Langmuir adsorption constant was obtained while analyzing the isotherm data at the equilibrium. These findings show that the combination of in situ quartz crystal microbalance measurements and models of adsorption can provide fundamental information about the adsorption of nanoparticles onto planar surfaces, which is extremely important for nanoparticle applications, where possible environmental concerns, such as the issues related to nanoecotoxicology and biological risks should arise.

Regarding the monitoring "in situ" of LbL assembly by QCM, the IONP dispersion and polyelectrolyte are introduced alternately into the QCM cell, to mimics the LbL procedure. Kim et al. measured the deposited mass of two bilayers of PSS/IONP [58]. Afterwards, Alcantara et al. monitored in situ the adsorption of cobalt ferrite nanoparticles

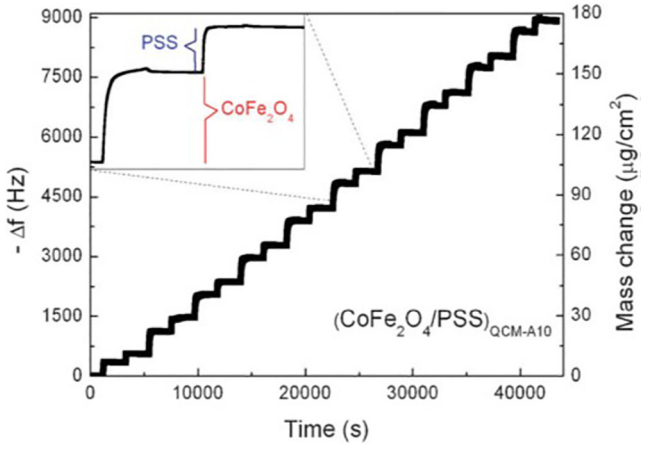

Fig. 2. Deposition of multilayered films of $(CoFe_2O_4/PSS)_{QCM\text{-}A10}$ monitored by QCM for a time window larger than eleven hours. Magnetic dispersion and polyelectrolyte were introduced alternately into the QCM cell (in situ), which mimics a LbL procedure. The inset indicates individual adsorption steps [66].

and sulfonated polystyrene ($CoFe_2O_4$/PSS) inside the QCM, using a $CoFe_2O_4$ colloidal dispersion expressed in mols of cobalt ferrite per liter of 8.9×10^{-6} mol L^{-1}, for a time window larger than eleven hours, see Fig. 2 [66]. Note that in a few minutes the adsorption of each component reaches equilibrium as expected for an electrostatic based process. The zoom of adsorption isotherms of each component are exhibited in the insert. This periodic behavior is ensured by the reversal of the net surface charge after complete adsorption of each layer, as previously discussed. The asymptotic form of isotherms suggests the occurrence of a first order kinetics process [66].

The first monolayer of IONPs adsorbed in glass substrate can be monitored through tapping-mode AFM images. In this mode, the sample is scanned by an oscillating probe whose oscillation amplitude is sensitive to both topography and mechanical properties of the sample surface. It can be performed when the immersion time of the substrate in the MF is short, i.g., 10 s, (see Fig. 3). A few individual nanoparticles and agglomeration of them are also observed. Spherical structures in AFM phase image (Fig. 3(B)) coincide with the features of the topography image (Fig. 3(A)). As the immersion time increases to 180 s, the surface is completely covered by nanoparticles nuclei with an increase in the number of adsorbed nanoparticles, as well as a larger number of agglomerates is also observed [67]. Since individual nanoparticles can be observed at short immersion times, it can be inferred that agglomerates are formed at the substrate surface, probably due to a nucleation process, rather than in the IONP colloidal suspension. Despite of the electrostatic imposed by their positive surface charges, dipolar interactions overcome repulsion among nanoparticles.

3. Nanocomposite properties

3.1. Nanocomposite structure and morphology

The surface morphology of nanocomposites can be investigated by tapping-mode AFM and by scanning electron microscopy (SEM). Fig. 4(A) presents typical SEM image of $(PANI/IONP)_{10}$, attained for the as prepared sample, due to the presence of the conducting polymer, PANI. It can be observed the uniformity of the surface morphology, showing no regions composed by only particles separated from polymer, with no phase segregation of nanoparticles and polymer. Additionally, Fig. 4(B) displays AFM topography of LbL film of $(IONP/PSS)_{10}$. A globular morphology is observed, which is basically composed of spherical IONP distributed over the entire nanocomposite surface, with no detectable phase segregation and arranged as a densely packed layer. Usually, LbL assembled IONP/polymer are absent of interlayer boundaries because polyelectrolyte chains tend to interpenetrate along the film stacking axis. Therefore, the nanocomposite contains similar fractions of each material and no interlayer boundaries are observed, which is in agreement with SEM image. Stratification of a LbL structure comprising IONP and poly(diallyldimethylammonium bromide), PDDA, was obtained with montmorillonite clay [57]. In this approach, it was found that montmorillonite produces a dense layer of overlapping aluminosilicate sheets, isolating one IONP layer from another. Magnetic and optical properties of these LbL nanocomposites were investigated [57]. Recently, the control of the horizontal and vertical coupling between individual 3-aminopropyl-trimethoxysilane modified magnetite nanoparticles LbL assembled with inorganic nanosheets of layered double hydroxides (LDH) was investigated. The tuning of the inter-magnetic- nanoparticle distance in both directions is induced by the control of charge density and thickness of LDH nanosheets. This approach has been employed to prepare highly anisotropic magnetic films [74].

Estimation of the nanocomposite film thickness can be performed by AFM technique. In order to create a step, the AFM tip is used to scratch and peel out a small spot of the nanocomposite deposited onto the solid substrate, which allows estimation of the sample thickness [95]. A linear dependence of the nanocomposite film thickness on the number of nominal PANI/IONP bilayers was found. It demonstrates that the cycling assembly process produces an increasing adsorption of PANI

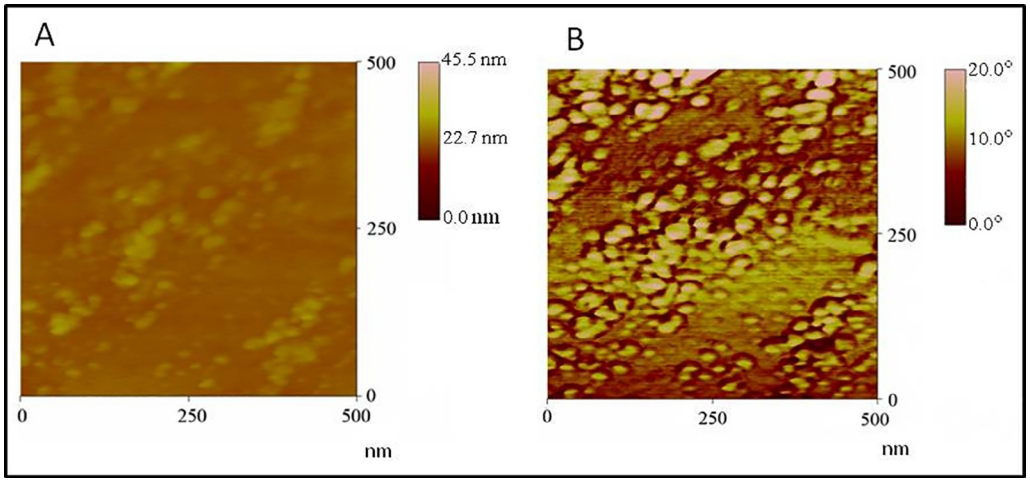

Fig. 3. Topography (A) and phase (B) AFM images of $CoFe_2O_4$ nanoparticles adsorbed onto a glass slide after a single immersion into a high diluted $CoFe_2O_4$ nanoparticle based magnetic fluid, for 10 s [67].

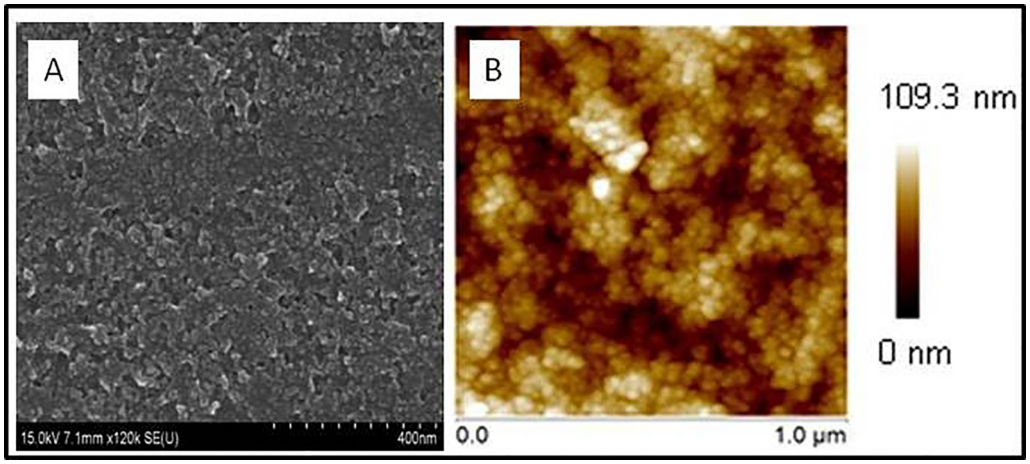

Fig. 4. SEM image of $(PANI/IONP)_{10}$ (A); and Topography AFM of $(IONP/PSS)_{10}$ nanocomposites (B). (b) [75].

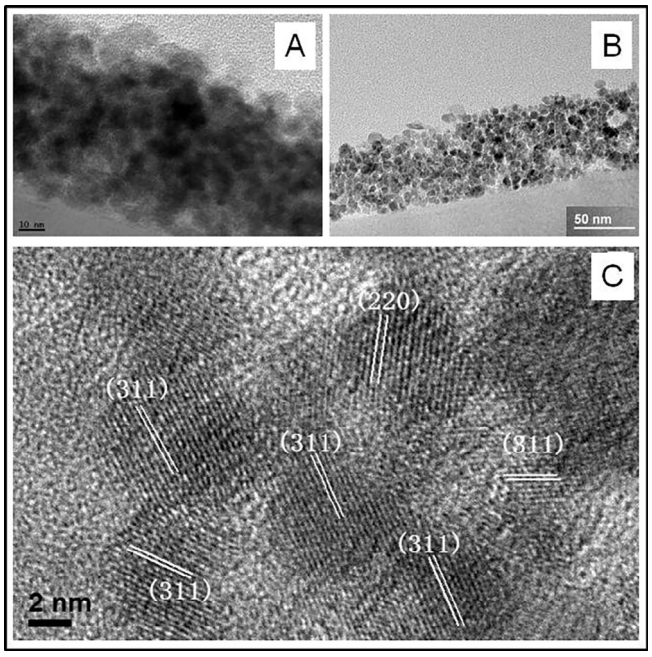

Fig. 5. Cross-sectional images for (A) $(PANI/\gamma\text{-}Fe_2O_3)_{A\text{-}10}$ and (B) $(PANI/\gamma\text{-}Fe_2O_3)_{B\text{-}10}$. (C) A high-resolution TEM image of maghemite nanoparticles embedded within the nanocomposite in (B) [70]. Scale bars: 10 nm (A); 50 nm (B); 2 nm (C).

and cit-MAG with fine control of film thickness and structure [62]. The thickness of nanocomposites can also be measured through cross-sectional TEM micrographs. Fig. 5(A) and (B) display HRTEM cross sectional images of nanocomposites with different concentrations of IONP in the colloidal dispersion employed as source of NP (2×10^{-3} g $L^{-1}$of $\gamma\text{-}Fe_2O_3$ for $(PANI/(\gamma\text{-}Fe_2O_3)_{A\text{-}10}$ and 2×10^{-4} g L^{-1} of γ-Fe2O_3 for $(PANI/(\gamma\text{-}Fe_2O_3)_{B\text{-}10})$. Lattice fringes in Fig. 5(C) were indexed as planes of (2 2 0) and (3 1 1) of a $\gamma\text{-}Fe_2O_3$ phase [70]. In Fig. 5(B), it is easily observed that $\gamma\text{-}Fe_2O_3$ nanoparticles homogeneously spread in the nanofilm while dressed by a tinny layer of PANI (brighter layer), which keeps nanoparticles isolated from each other. The amount of $\gamma\text{-}Fe_2O_3$ nanoparticles encapsulated within the nanofilm A is higher because of the higher concentration of $\gamma\text{-}Fe_2O_3$ nanoparticles in the MF sample A employed for its deposition. Thicknesses of both nanofilms are about 60 nm which is consistent with the values previously recorded by AFM [70]. An evolution of the cross sectional TEM micrographs of PANI/$\gamma\text{-}Fe_2O_3$ nanocomposites with increasing number of bilayers, reveals a systematic reduction of the average particle–particle distance within the hosting polymer [70]. Grigoriev et al. investigated the structure and surface morphology of LbL nanocomposites monitoring their assembly through AFM, UV–vis spectroscopy, and ellipsometry. The dependency of the real part of the complex refractive index, thickness, roughness, and optical absorbance of the films, on the number of bilayers, and their interrelations with the nanocomposite structure were discussed in the Ref. [60].

The finger print phase of IONP in nanocomposites can be unequivocally probed by micro Raman spectroscopy. As for instance, even in very thin LbL structures, the Raman spectrum of the nanocomposite comprising only 3 bilayers ($(IONP/PSS)_3$), excited with argon ion laser (λ = 514 nm), displayed in Fig. 4, shows characteristic features of magnetite [75]. To minimize degradation, this spectrum was recorded at the lowest laser excitation, 0.3 mW [96]. Raman modes were identified from data available in the literature considering the characteristic vibrational modes of the cubic spinel: T_{2g}^1 for 193 cm^{-1}, E_g for 306 cm^{-1}, T_{2g}^2 for 450–490 cm^{-1}, and T_{2g}^3 for 538 cm^{-1}, and A_{1g} for 668 cm^{-1}, for Fe_3O_4 single crystal, describing normal mode motions of the FeO_4 tetrahedron [97].

After the fitting procedure of the Raman spectrum (Fig. 6) performed with Lorentzian-like components, it was found the presence of five peaks, at 189 ($T_{2g}(1)$), 328 (E_g), 470 ($T_{2g}(2)$), 540 ($T_{2g}(3)$) and 670 (A_{1g}) cm^{-1}, characteristics of magnetite phase [97]. Further, the presence of the polymer PSS encapsulating IONP preserves the magnetite phase against laser irradiation during micro Raman experiments. Otherwise, in the case of the magnetite powder sample, submitted to

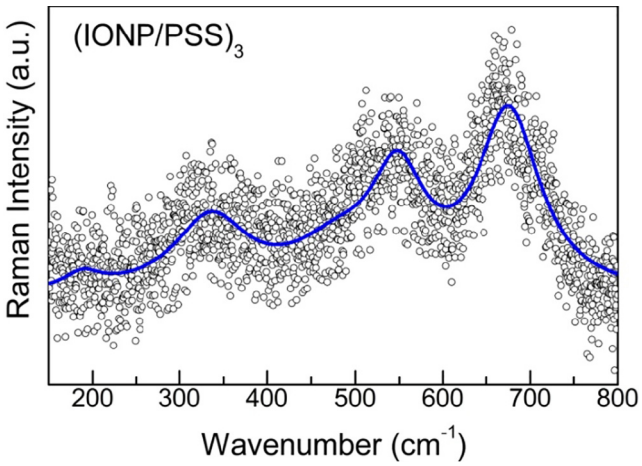

Fig. 6. Room temperature Raman spectrum of $(IONP/PSS)_3$ nanocomposite sample excited with argon ion laser (λ = 514 nm) [75].

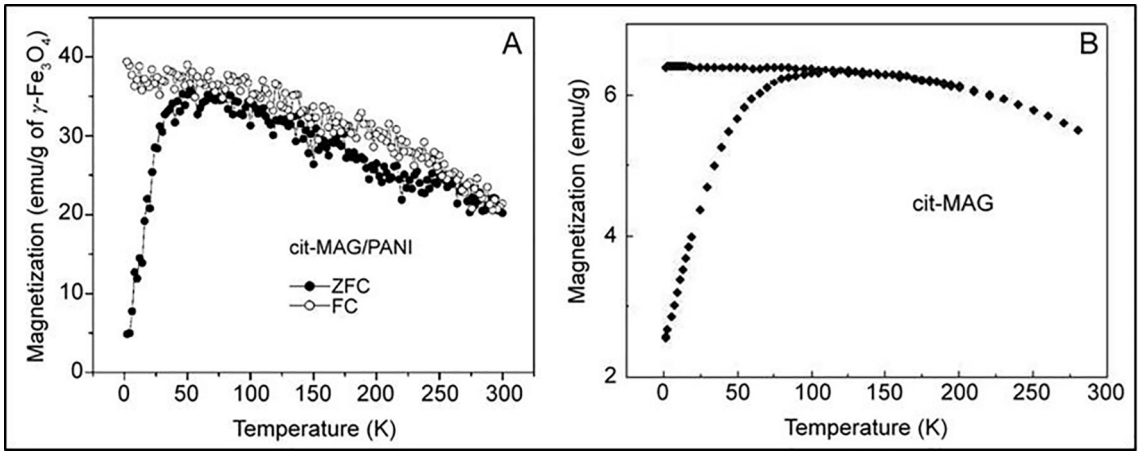

Fig. 7. ZFC-FC curves obtained with a DC field of 100 Oe (A) cit-MAG/PANI nanocomposite film containing 50-bilayers and (B) cit-MAG powder sample [62].

the same measurements conditions, its Raman spectrum displays also characteristic bands of maghemite, indicating some level of oxidation [75].

UV–vis spectroscopy, QCM data and AFM images, show that the successive dipping of substrates into cationic IONP dispersions/anionic polyelectrolyte solutions, or anionic IONP and cationic polymers, as shown in Scheme 1, results in a constant increase on the adsorbed amount of each component and respective layer thickness. This behavior is highly reproducible from sample to sample provided that physicochemical conditions of deposition, for example nanoparticles' and polyelectrolytes' concentrations have been previously established. These nanocomposite characteristics can be improved further by performing the LbL assembly with the assistance of an automated system [98].

3.2. Magnetic properties

IONP/polymer nanocomposites can display collective magnetic properties arising from inter-particle interactions [99]. The magnetic interaction between particles is connected with a specific structural conformation of the nanocomposite. Therefore, the relative importance of these contributions can be tuned experimentally to some extent by changing the nanocomposite characteristics, such as particle-size, degree of polydispersity, magnetic anisotropy, and average interparticle distance, as well as nanocomposite morphology. In particular, dipolar interactions can play a significant role in macroscopic behavior of magnetic nanocomposites [100–102].

Concerning LbL assemblies, nanoparticle interactions depend on particle and polymer characteristics, as well as particle spatial distribution inside the matrix. The fine tuning of structure thickness and average particle-particle distance within the nanocomposite can be attained by varying the number of bilayers (IONP/polymer) or via changing the concentration of particles within the colloidal dispersion used as source of nanoparticle in LbL deposition [62,69]. Therefore, the simulation of real three dimensional systems to predict the magnetic response of an ensemble of interacting magnetic nanoparticles is mandatory to understanding the relationship between the nanocomposite structure and the end magnetic properties.

Experimental investigations comprising field- and temperature-dependence of magnetization and susceptibility of LbL nanocomposites have been performed. Initially, Aliev et al. studied the effect of silica coated IONP LbL assembled on the interparticle interaction, and its effect upon magnetic properties through field-dependence of magnetization and field and temperature dependence of susceptibility measurements. As a control sample, they prepared nanocomposites with uncoated IONP. According with their findings a reduction of the cooperative magnetization switching between adjacent NPs occurred, due to the presence of the insulating silica shell [55]. Kim et al. investigate the LbL assembly of IONP and PSS, performing a detailed characterization on the nanocomposite structure. Regarding magnetic properties, the magnetization versus applied field attained from nanocomposite sample comprising two bilayers of IONP/PSS showed the same behavior of pure IONPs [58]. Experiments conducted afterwards showed that the superparamagnetic behavior of the iron oxide nanoparticles is maintained after their LbL assembly with either conducting or not conducting polymer matrixes [58,64,70]. The magnetic properties of stratified LbL structures comprising IONP and PDDA obtained with montmorillonite clay, were compared with similar structures comprising only IONP and the polymer [57]. The authors attributed the differences between magnetic properties of assemblies with different architectures to the insulation effect of the clay layers inserted between IONP layers. The authors claim that the montmorillonite sheets disrupt the electron exchange interactions between the magnetite nanoparticles in adjacent layers, thus limiting the magnetization reversal to two dimensions [57]. The presence of IONP in LbL structures – comprising a polymer and a dispersion of colloidal IONP added to poly(o-ethoxyaniline) (POEA) solution – was accessed through ZFC and FC curves of nanocomposites with 30 bilayers. This procedure gives also an indication of the order of magnitude of the mean radius of IONPs [61]. Pichon et al. studied the magnetic properties of LbL assembled monodisperse IONP with PAH, by comparing samples with different architecture obtained with IONP layers separated by bilayers of PAH/PSS [68]. They found that NPs interact preferentially in the plane of the IONP layers through dipolar interactions. Moreover, they also conclude that the resulting strong magnetic anisotropy along each IONP layer induces their antiparallel coupling, the later being dependent on the dipolar interactions occurring between NPs of adjacent layers [68].

In nanoparticulated magnetic systems, the zero-field-cooled (ZFC)/field-cooled (FC) magnetizations are sensitive to the size, morphology, and particle-particle interaction [103]. The ZFC/FC curves (DC probing field of 100 Oe) of the cit-MAG/PANI nanocomposite film containing 50-bilayers and of cit-MAG powder sample are presented in Fig. 7 (A) and (B), respectively. The estimated blocking temperature (T_B) for the powder sample was ~80 K, while for $(cit\text{-}MAG/PANI)_{50}$ was ~40 K. It is observed a reduction of T_B from the IONP powder to the nanocomposite, that can be attributed to the fact that cit-MAG nanoparticle is enveloped by the polymer, as observed in Fig. 5(B). Attained K_B values are in agreement with the observed behavior of the magnetization curves, which did not presented coercivity above these temperatures [62]. However, the ZFC curve does not exhibit the typical Curie-Weiss behavior above 40 K. The authors attributed this deviation to the particle-particle interaction. Values of T_B obtained from the recorded ZFC/FC curves using the cit-MAG/PANI nanocomposite films comprising 5-, 10-, 25-, and 50-bilayers were 30, 35, 39, and 40 K, respectively. The

monotonic increase of T_B with the number of deposited bilayers indicates that interactions among nanoparticles increase the more cit-MAG are incorporated within the nanocomposite. When nanosized magnetic particles are brought close together the magnetic interaction (dipole and/or exchange interaction) will affect the superparamagnetic relaxation.

Theoretical and phenomenological studies proposed – to account for nanosized magnetic particle-particle interaction – predict an increase of the blocking temperature as the single particle anisotropy energy barrier increases with the interparticle interaction [104–106]. For the case of cit-MAG/PANI system, AFM images revealed that immersion of the PANI-coated substrate into the magnetic fluid sample led to a dense layer of cit-MAG and some aggregates, which could contribute toward the increase of the nanoparticle interaction. As the multilayer deposition proceeds, more nanoparticles are incorporated within the nanocomposite and nanoparticle densification occurs, with nanoparticles being accommodated into the voids left by previous layers, as observed in HRTEM cross sectional images (see Fig. 5). In addition, the system's dynamic behavior from the temperature dependence of the ac magnetic susceptibility components (in-phase (χ') and out of-phase (χ'') was investigated, in the frequency range of $100 < f < 10^4$ Hz [70]. The temperature dependence of the imaginary part of the ac susceptibility, $\chi''(T)$, of the PANI/γ-$Fe_2O_3)_A$ nanofilms reveals an increase of T_B as the number of bilayers increases, as shown in Fig. 8(A). The ac magnetic susceptibility of nanosized magnetic particles (noninteracting systems) has been described by models proposed by Dormann et al. [107] and Gittleman et al. [108]. For these systems, the time required for magnetic moment reversal along the easy magnetization axis follows an Arrhenius-like behavior governed by $\tau = \tau_o \exp \Delta E/k_B T$, where τ_o is the microscopic magnetic relaxation time (related to the reversal attempt frequency), ΔE is the effective energy barrier, k_B is the Boltzmann constant and T is the absolute temperature. From the maxima of $\chi''(T)xT$ curves, at each measuring frequency (f), Arrhenius plots ($\log \tau x T^{-1}$) were obtained, from which ΔE and τ_o were extracted [69].

Fig. 8(B) shows that ΔE systematically increases and tends to saturate as the number of bilayers increases from 5 to 50. This increase in ΔE was attributed to film densification, which implies in shortening the particle-particle distance and, consequently, enhancing the particle-particle dipolar interaction. Furthermore, the estimated $\Delta E/k_B$ value for the PANI/γ-Fe_2O_3 nanofilms are rather high, compared with typical values found in non interacting magnetic nanoparticles where a thermal-activated magnetic relaxation process follows an Arrhenius law [109]. Furthermore, only the (PANI/γ-$Fe_2O_3)_{A\text{-}5}$ nanofilm presented $\tau_o$value within the range of noninteracting superparamagnetic particles.

In summary, the results attained from magnetic measurements about the behavior of the blocking temperature, effective energy barrier, and the microscopic magnetic relaxation time, as a function of the number of bilayers of PANI/γ-Fe_2O_3 nanocomposites (from 5 to 50), evidenced the occurrence of dipolar interactions. Simulations of the as-produced samples were performed to assess both the nanocomposite's morphology and the corresponding magnetic signatures using the cell dynamic system (CDS) [110] approach and Monte Carlo (MC), respectively. MC simulations were developed through the standard Metropolis algorithm. In a first step of the multistage simulation procedure, the distribution of particles within the hosting matrix was attained by means of the CDS model. The 3D structure provided by the CDS step was further employed in a Monte Carlo (MC) simulation of zero-field-cooled/field-cooled (ZFC/FC) and magnetic hysteresis loops (M x H curves) for the system. These simulations were aimed to draw a realistic picture of the as-produced ultra-thin nanocomposites comprising maghemite nanoparticles dispersed in polyaniline.

The $(PANI/cit\text{-}MAG)_n$ nanocomposite film is a typical binary system composed by nanosized magnetic particles embedded within the polymeric matrix, as observed in the cross-sectional micrograph of a $(PANI/cit\text{-}MAG)_{B\text{-}10}$ sample containing ten (n = 10) bilayers (Fig. 5(B)). This binary material system was idealized by an array of individual and

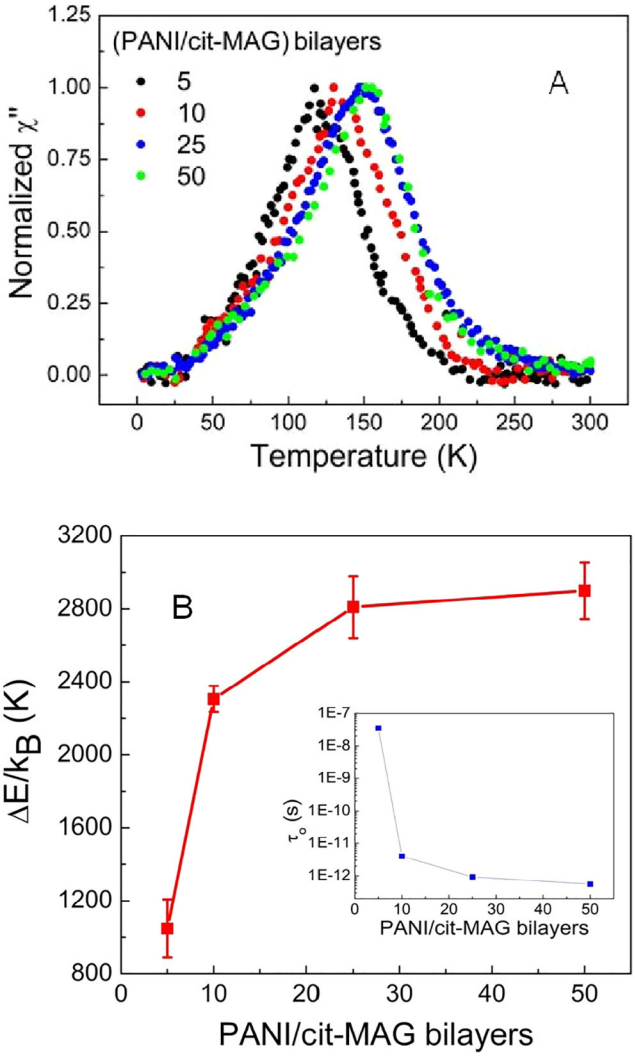

Fig. 8. Imaginary χ'' component of the ac susceptibility (A) and effective energy barrier (B) of $(PANI/\gamma\text{-}Fe_2O_3)_{A\text{-}n}$ samples with different number of bilayers (n = 5, 10, 25 and 50 bilayers). The inset of (B) shows the obtained values of τ_o using the Arrhenius relation. Symbols are experimental points, whereas solid lines are guide to the eyes [70].

isolated spheres, with a well-defined average radius and size distribution, packed in a local HCP order but presenting long-range disorder. The real sample was prepared from a colloidal suspension composed by monodomain nanosized particles (cit-MAG), with average diameter D_{TEM} = 7.5 nm determined by TEM. Fig. 9 shows the simulated cross-section IONP/polymer structure after CDS modeling. It is important to point out that the simulated is solely generated by the algorithm [72].

To simulate the nanocomposites with increasing thickness, nanoparticles were arranged within three hypothetical ultrathin slabs of increasing thickness: S1 (541.9 nm × 541.9 nm × 27.1 nm), S2 (338.5 nm × 338.5 nm × 33.9 nm), and S3 (233.9 nm × 233.9 nm × 36.0 nm). Such arrangements provided quasi-2D structures with different particle–particle distances. Particles with lognormal diameter distribution centered at D = 7.5 nm were considered in this simulation. After 2,000 iterations, the simulated pair distribution function, g(r), attained for each slab indicates a short-range order, characterized by the presence of a first peak located at R_{S1} = 12 nm, R_{S2} = 10 nm and R_{S3} = 8 nm, respectively. In real samples, these values represent the nearest-neighbor particle distance (center-to-center). The pair distribution function, g(r), attained by the CDS simulation (Fig. 10 (B)) clearly indicates the nanoparticles' ensemble has a short-range order at

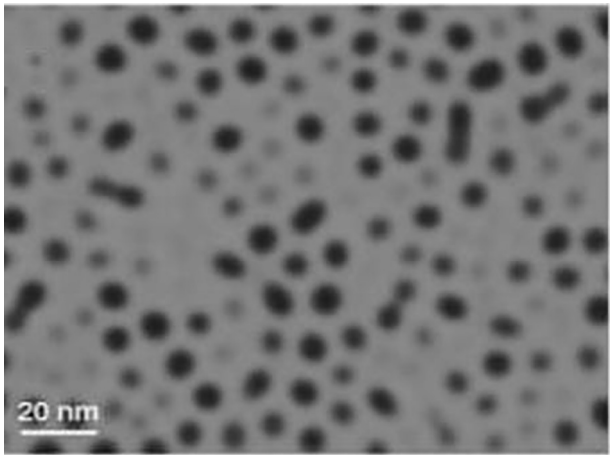

Fig. 9. Cross-section IONP/polymer structure after CDS modeling [72].

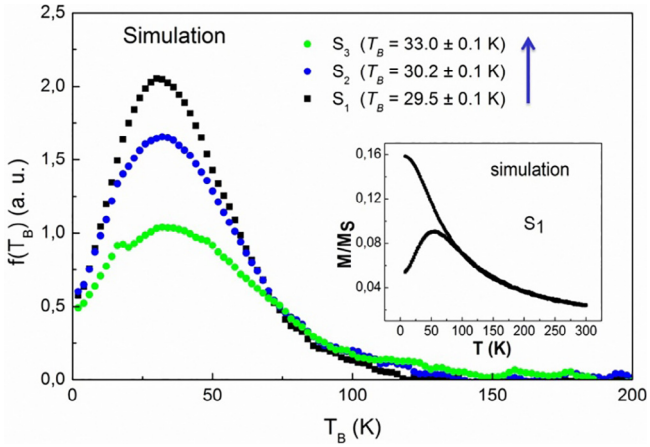

Fig. 11. Blocking temperature distribution functions determined from the simulated ZFC/FC curves at a field of 100 Oe. Simulations were performed for the three slabs, as indicated. The inset shows the simulated ZFC/FC curves for the slab S1 [70].

distances shorter than 30 nm. From the first g(r) peak position (see Fig. 10(B)) one determines the average center-to-center nearest neighbor distance (R_{nn}) equal to 10 nm [72]. The correspondent experimental value determined from HRTEM images as observed in the inset of Fig. 10(A) is also 10 nm. It appears that morphological features simulated by the CDS model correlate quite well to those presented by the real sample HRTEM micrographs.

After the CDS simulation the values of order parameter for all cells were extracted. Afterwards, this information was converted into Np sets of parameters $\{\vec{r_i}; \vec{m_i}; K_i^S; \hat{e}_i^S\}$ defined as position ($\vec{r_i}$), total magnetic moment ($\vec{m_i}$), shape anisotropy constant (K_i^S) and easy magnetization axis ($\hat{e}_i^S$) of the i-th nanoparticle [72].

In the CDS simulated ensemble the distance Rnn between nearest neighboring grains is relatively large, so that direct exchange and RKKY interactions were neglected. Within this approximation, the magnetic dipolar interaction was the only one considered in the energy terms to take into account in the MC simulation. These simulated magnetic structures (slabs S1, S2 and S3) were then employed in the Monte Carlo simulation of ZFC/FC curves using the standard Metropolis algorithm with angular-restricted steps (θ_{max}=15°) [111,112]. The total energy of the Np particles in the presence of an external magnetic field included the energy of particles due the external applied field (H), shape (K^S) and crystalline (K^c) anisotropies, and dipolar energy contributions. [72]. Using this approach, the ZFC/FC curves were simulated for H_{DC} = 100 Oe (in plane) at a rate of 50 MCS/2 K, where MCS refers to MC steps. The simulated distribution of T_B values is shown in Fig. 11 and represents the averages of more than 2,000 independent realizations. The inset in Fig. 11 shows the simulated ZFC/FC curves for the slab S1. Note that the T_B values obtained from the curves shown in Fig. 11 systematically increase from the thinner (S1, T_B = 29.5 K) to the thicker (S2, T_B = 30.2 K and S3, T_B = 33 K) slabs, as observed in the T_B values attained for the fabricated PANI/γ-Fe_2O_3 nanofilms. This finding represents a strong support to the hypothesis that both blocking temperature and effective energy barrier for magnetic moment reversal increase as the PANI/γ-Fe_2O_3 nanofilms become thicker and denser, as the particle–particle distance decreases and, consequently, the dipolar interaction becomes stronger.

Recently, Shi et al. investigated the magnetic properties (coercivity and saturation magnetization) of the (APTS-Fe_3O_4/LDH)n composites as a function of interparticle distance, in the horizontal and vertical

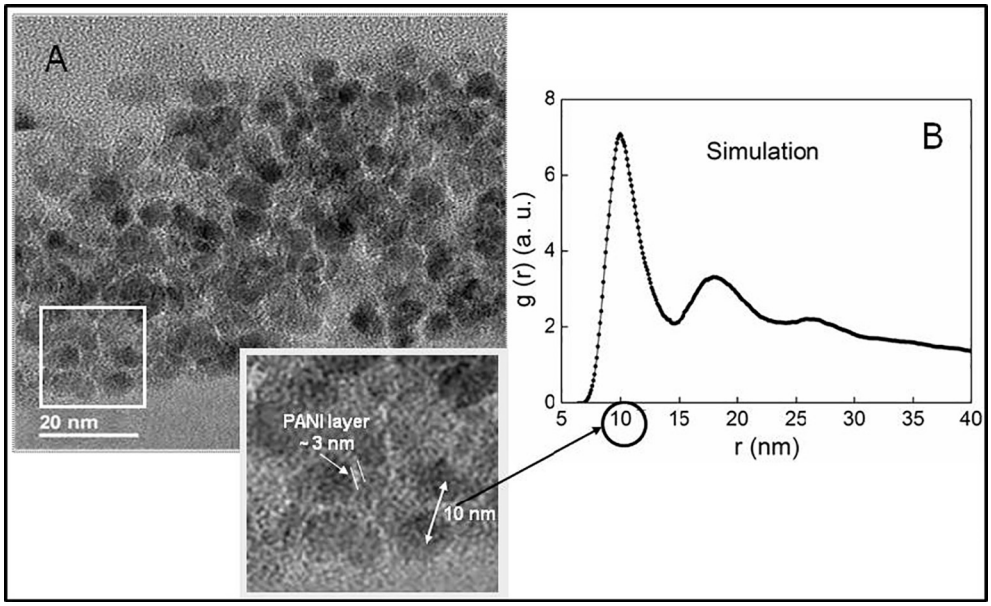

Fig. 10. HRTEM cross sectional image of IONP/PANI sample (A) the inset shows the experimental average center-to-center nearest neighbor distance. The pair distribution function, g(r), attained by the CDS simulation (B) indicates the average center-to-center nearest neighbor distance equal to 10 nm [72].

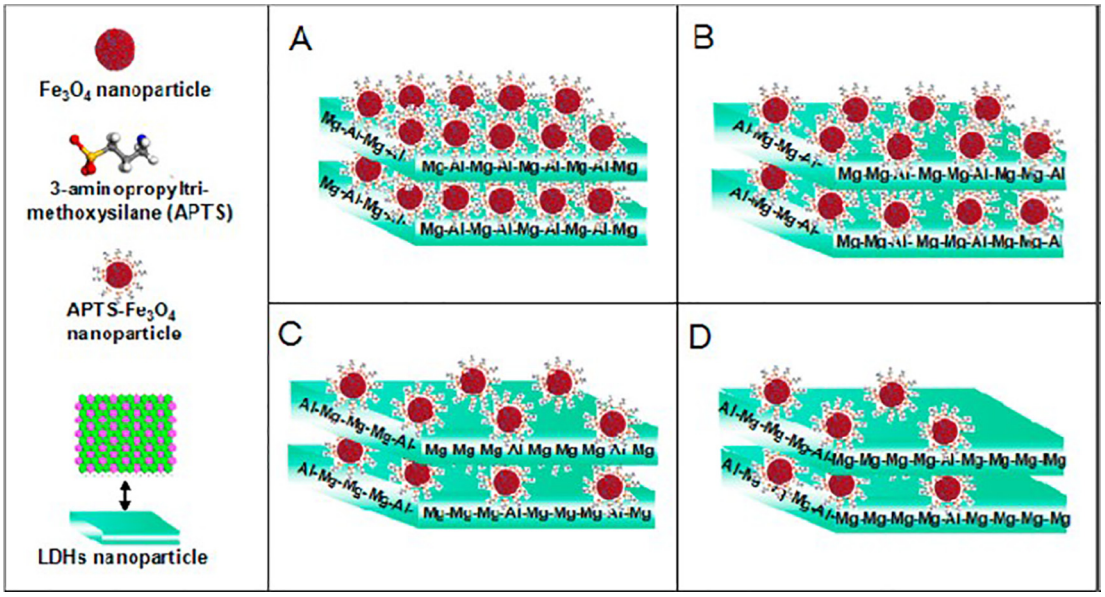

Scheme 2. Illustration of the assembly and structure of the $(APTS\text{-}Fe_3O_4/LDH)_2$ films and the effect of changing the composition (and charge) of the Mg_XAl-LDH material: (A) x = 1 and t = 0 h, (B) x = 2 and t = 0 h, (C) x = 3 and t = 0 h, and (D) x = 4 and t = 0 h. Reprinted from [74].

directions. The nanocomposité morphology was modulated by controlling the charge density and layer thickness of layered double hydroxides (LDH) - $Mg_xAl\text{-}NO_3$ LDH (x = 1, 2, 3, and 4) nanosheets [74]. Scheme 2 illustrates the assembly and structure of the $(APTS\text{-}Fe_3O_4/LDH)_2$ films and the effect of changing the composition (and charge) of the Mg_XAl-LDH material: (A) x = 1 and t = 0 h, (B) x = 2 and t = 0 h, (C) x = 3 and t = 0 h, and (D) x = 4 and t = 0 h. The magnetic hysteresis loops for the $(APTS\text{-}Fe_3O_4/LDH)_{35}$ films (x = 1, 2, 3, and 4) measured at room temperature showed that all samples exhibit the superparamagnetic behavior with negligible coercivity (*Hc*). They found that the $(APTS\text{-}Fe_3O_4/LDH)_{35}$ films (x = 1, 2, 3, and 4) display noncoincident hysteresis loops in the parallel and perpendicular directions of magnetic field, compared to the coincident curves of the Fe_3O_4 and $APTSFe_3O_4$ nanoparticles, indicating magnetic anisotropy of nanocomposites. Further, *Hc* value in the parallel direction is more than 3-folds higher than that in the perpendicular direction, but the saturation magnetization in the parallel direction is only ~80% of the perpendicular one. The authors claim that the rigid and oriented LDH nanosheets induced ordered alignment of the spherical Fe_3O_4 nanoparticles, resulting in magnetic anisotropy property of nanocomposites [74].

4. Applications

The potential of novel LbL architectures (thickness 50–90 nm), comprising cobalt ferrite nanoparticles (np-$CoFe_2O_4$) and polyelectrolytes (sulfonated lignin – SL, poly(3,4-ethylenedioxy) thiophene:polystyrene sulfonic acid – PEDOT:PSS, and Polyaniline – PANI), for chemical sensing and energy storage, was evaluated by impedance spectroscopy [113] while they were exposed to room air, or immersed into ultra-pure water or diluted NaCl aqueous solution [24,25]. Three types of nanocomposite architectures were assembled on top of interdigitated microelectrodes (IMEs): film-I (control): $(PANI/SL)_{10}$; film-II $(np\text{-}CoFe_2O_4/PEDOT:PSS)_{10}$ and film-III: $(PANI/SL/np\text{-}CoFe_2O_4/SL)_5$, as illustrated in Scheme 3. Impedance data were further fitted with equivalent circuit models from which individual contributions of particle's bulk and interfaces to the charge transport within the nanocomposites could be evaluated. They found that the charge transport across the polyelectrolyte/nanoparticle interfaces dominates the dielectric behavior of nanocomposite based on np-$CoFe_2O_4$ assembled LbL with different polyelectrolytes. The complex permittivity and the dissipation factor of these NCs are much smaller than those measured in pressed pellets made exclusively of np-$CoFe_2O_4$. Furthermore, they found evidences that such NCs display a synergistic dielectric behavior, different from that exhibited by their individual counterparts, much likely due to enlarged nanoparticle–polyelectrolyte interfaces. These findings enable these IONP structures to applications where energy dissipation has to be minimized, for example in capacitors [24].

Nanosized np-$CoFe_2O_4$ assembled onto IMES originates sensoactive materials for liquid media chemical sensors, due to the electrical insulating behavior and the enhanced interfacial area provided by IONP. These resulting NCs are sensitive to the presence of ions in solution, as indicated by fitting impedance data with the response of an equivalent circuit model [25].

LbL $(PANI/IONP@cit)_{20}$ nanocomposite film, assembled onto Indium-doped tin oxide (ITO) substrates, has been produced and tested as electrodes for supercapacitors. The electrochemical behavior of $(PANI/IONP@cit)_{20}$ structures as working electrode was investigated by cyclic voltammetry and chronopotentiometry in a three-electrode configuration cell (reference electrode: Ag/AgCl; counter electrode: Pt) in $0.5\,mol \times L^{-1}$ Na_2SO_4 as the electrolyte solution. They found that this low-cost structure is promising candidate for potential application as electrodes for supercapacitors [76].

5. Conclusions

In this review we have summarized some recent progress on design and assembly of hybrid nanoscale composites consisting of iron oxide superparamagnetic nanoparticles and polymers prepared by LbL. The LbL concept, the characterization techniques, the influence of the deposition parameters, the physical properties of the nanocomposites, and some of their applications have also been addressed. The IONP materials can be LbL assembled due to electrostatic interactions. In addition, their composition and structure can be fine tailored. The internal structure of the resulting nanocomposites features individual particles enclosed by an extremely thin layer of polymers, as observed in cross-sectional TEM images and further confirmed by electrical measurements. Hence the respective nanocomposite films exhibit a synergistic dielectric behavior quite different from that of their individual components. This unique feature, rarely observed in nanocomposites obtained by other physical or chemical methods, opens up opportunities for their applications in sensors and other devices such as capacitors in

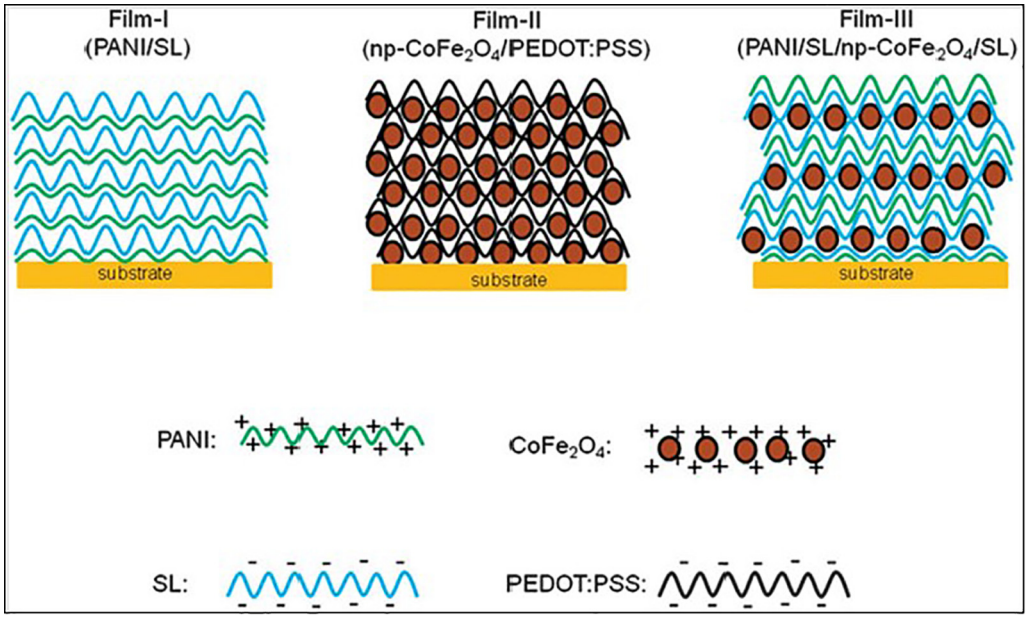

Scheme 3. Illustration of different nanocomposite architectures and materials employed in the depositions [24].

which energy dissipation has to be minimized.

Nanocomposite morphology can be simulated using the CDS. These 3-D simulated morphologies can serve as an input data to perform Monte Carlo simulation of magnetic properties of these nanocomposites. The computational results are in good agreement with cross-sectional HRTEM images, and magnetic measurements (MxH and ZFC/FC), indicating that nanoparticles LbL assembled present some level of interaction that can be modulated by deposition conditions. Moreover, the interparticle dipolar interactions can be tuned by controlling the IONP concentration of the magnetic colloidal dispersion, by changing the number of bilayers (thickness) and NC architecture [68–72,74], opening-up possibilities to produce ferrite nanoscale magnetic materials with tailored characteristics.

Acknowledgements

The financial support from the Brazilian agencies MCT-CNPq, FINEP, FAP-DF, FINATEC and CAPES is gratefully acknowledged. Thanks to Professor Fanyao Qu, Instituto de Fisica, Universidade de Brasilia, Brazil, for helpful comments and discussions. Thanks to Professor Steve Granick, University of Illinois at Urbana-Champaign, United States, and CAPES-Brazil (4410-08-4), to provide access to the Frederick Seitz Material Research Laboratory facilities, and to Dr. J. G. Wen (Electron Microscopy Center, Materials Science Division, Argonne National Laboratory, Argonne, Illinois, United States) for the support in the TEM measurements.

References

[1] M. Grzelczak, J. Vermant, E.M. Furst, L.M. Liz-Marzán, Directed self- assembly of nanoparticles, ACS Nano 4 (7) (2010) 3591–3605.
[2] A.C. Balazs, T. Emrick, T.P. Russel, Nanoparticle polymer composites: where two small worlds meet, Science 314 (2006) 1107–1110.
[3] K.J. Si, Y. Chen, Q. Shi, W. Cheng, Nanoparticle superlattices: the roles of soft ligands, Adv. Sci. 5 (2018) 1700179.
[4] S. Imai, Y. Hirai, C. Nagao, M. Sawamoto, T. Terashima, Programmed self-assembly systems of amphiphilic random copolymers into size-controlled and thermoresponsive micelles in water, Macromolecules 51 (2) (2018) 398–409.
[5] M. Shahrousvand, M.S. Hoseinian, M. Ghollasi, A. Karbalaeimahdi, A. Salimi, F.A. Tabar, Flexible magnetic polyurethane/Fe_2O_3 nanoparticles as organic-norganic nanocomposites for biomedical applications: properties and cell behavior, Mater. Sci. Eng., C 74 (2017) 556–567.
[6] J.T. O'Neal, M.J. Bolen, E.Y. Dai, J.L. Lutkenhaus, Hydrogen-bonded polymer nanocomposites containing discrete layers of gold nanoparticles, J. Colloid Interface Sci. 485 (2017) (2017) 260–268.
[7] D. Toulemon, D.M.V. Rastei, D. Schmool, J.S. Garitaonandia, L. Lezama, X. Cattoën, S. Bégin-Colin, B.P. Pichon, Enhanced collective magnetic properties induced by the controlled assembly of iron oxide nanoparticles in chains, Adv. Funct. Mater. 26 (2016) 2454–2462.
[8] A.P. Alivisatos, Semiconductor clusters, nanocrystals, and quantum dots, Science 271 (1996) 933–937.
[9] P.T. Hammond, Form and function in multilayer assembly: new applications at the nanoscale, Adv. Mater. 16 (2004) 1271–1293.
[10] M. Ferreira, M.F. Rubner, Layer-by-layer manipulation of conjugated polyions, Macromolecules 28 (1995) 7107–7114.
[11] Y. Lvov, K. Ariga, I. Ichinose, T. Kunitake, Assembly of multicomponent protein films by means of electrostatic layer-by-layer adsorption, J. Am. Chem. Soc. 117 (1995) 6117–6123.
[12] Y. Lvov, Z.Q. Lu, J.B. Schenkman, X.L. Zu, J.R. Rusling, Direct electrochemistry of myoglobin and cytochrome p450(cam) in alternate layer-by-layer films with DNA and other polyions, J. Am. Chem. Soc. 120 (1998) 4073–4080.
[13] S.W. Lee, B.S. Kim, S. Chen, Y. Shao-Horn, P.T. Hammond, Layer-by-layer assembly of all carbon nanotube ultrathin films for electrochemical applications, J. Am. Chem. Soc. 131 (2009) 671–679.
[14] D.W. Lee, T.-K. Hong, D. Kang, J. Lee, M. Heo, J.Y. Kim, B.S. Kim, H.S. Shin, Highly controllable transparent and conducting thin films using layer-by-layer assembly of oppositely charged reduced graphene oxides, J. Mat. Chem. 21 (2011) 3438–3442.
[15] C.Y. Jiang, S. Markutsya, V.V. Tsukruk, Collective and individual plasmon resonances in nanoparticle films obtained by spin-assisted layer-by-layer assembly, Langmuir 20 (3) (2004) 882–890.
[16] A.O.T. Patrocinio, L.G. Paterno, N.Y.M. Ilha, Role of polyelectrolyte for layer-by-layer compact TiO_2 films in efficiency enhanced dye-sensitized solar cells, J. Phys. Chem. C 114 (2010) 17954–17959.
[17] J.G. Santos, J.R. Souza, C.J. Letti, M.A.G. Soler, P.C. Morais, M.A. Pereira-da-Silva, L.G. Paterno, Iron oxide nanostructured electrodes for detection of copper(II) ions, J. Nanosci. Nanotechnol. 14 (2014) 6614–6623.
[18] M.A. Gross, M.J.A. Sales, M.A.G. Soler, M.A. Pereira-da-Silva, M.F.P. da Silva, L.G. Paterno, Reduced graphene oxide multilayers for gas and liquid phases chemical sensing, RSC Adv. 4 (2014) 17917–17924.
[19] G. Decher, Fuzzy nanoassemblies: toward layered polymeric multicomposites, Science 277 (1997) 1232–1237.
[20] N.A. Kotov, Layer-by-layer assembly of nanoparticles and nanocolloids: intermolecular interactions, structure and materials perspectives, in: G. Decher, J.B. Schlenoff (Eds.), Multilayer Thin Films, Wiley-VCH Verlag GmbH & Co. KGaA, Weinheim, 2002, pp. 207–270.
[21] K. Ariga, J.P. Hill, Q. Ji, Layer-by-layer assembly as a versatile bottom-up nanofabrication technique for exploratory research and realistic application, PCCP 9 (2007) 2319–2340.
[22] L.G. Paterno, M.A.G. Soler, Layer-by-layer enabled nanomaterials for chemical sensing and energy conversion, JOM 65 (2013) 709–719.
[23] S. Seo, S. Lee, Y.P. Park, Automatic layer-by-layer spraying system for functional thin film coatings, Rev. Sci. Instrum. 87 (2016) 036110.
[24] G.B. Alcantara, L.G. Paterno, F.J. Fonseca, M.A. Pereira-da-Silva, P.C. Morais, M.A.G. Soler, Dielectric properties of cobalt ferrite nanoparticles in ultrathin nanocomposite films, PCCP 15 (2013) 19853–19861.
[25] G.B. Alcantara, L.G. Paterno, F.J. Fonseca, M.A. Pereira-da-Silva, P.C. Morais,

M.A.G. Soler, Layer-by-layer assembled cobalt ferrite nanoparticles for chemical sensing, J. Nanofluids 2 (2013) 175–183.
[26] P.T. Hammond, Building biomedical materials layer-by-layer, Mater. Today 15 (2012) 196–206.
[27] M.A.G. Soler, L.G. Paterno, P.C. Morais, Layer-by-layer assembly of magnetic nanostructures, J. Nanofluids 1 (2012) 101–119.
[28] F.L. Leite, L.G. Paterno, C.E. Borato, P.S.P. Herrmann, O.N. Oliveira, L.H.C. Mattoso, Study on the adsorption of poly(O-ethoxyaniline) nanostructured films using atomic force microscopy, Polymer 46 (2005) 12503–12510.
[29] M.A.G. Soler, L.G. Paterno, Magnetic Nanoparticles, in: O.N. Oliveira Jr, M. Ferreira, A.L. Da Róz, F.L. Leite (Eds.), Nanostructures. Elsevier, 2017, pp. 147–186.
[30] T.F.O. Melo, S.W. da Silva, M.A.G. Soler, E.C.D. Lima, P.C. Morais, Investigation of surface passivation process on magnetic nanoparticles by Raman spectroscopy, Surf. Sci. 600 (2006) 3642–3645.
[31] M.A.G. Soler, E.C.D. Lima, E.S. Nunes, F.L.R. Silva, A.C. Oliveira, R.B. Azevedo, P.C. Morais, Spectroscopic study of maghemite nanoparticles surface-grafted with DMSA, J. Phys. Chem. A 115 (2011) 1003–1008.
[32] J. Philip, P.D. Shima, B. Raj, Nanofluid with tunable thermal properties, Appl. Phys. Lett. 92 (2008) 043108.
[33] S. Bedanta, W.J. Kleemann, Superparamagnetism, J. Phys. D Appl. Phys. 42 (2009) 013001.
[34] R. Singh, Unexpected magnetism in nanomaterials, J. Magn. Magn. Mater. 346 (2013) 58–73.
[35] J. Philip, J.M. Laskar, Optical properties and applications of ferrofluids—a review, J. Nanofluids 1 (2012) 3–20.
[36] S. Bagheri, N.M. Julkapli, Modified iron oxide nanomaterials: functionalization and application, J. Magn. Magn. Mater. 416 (2016) 117–133.
[37] M. Magnani, L. Galluzzi, I.J. Bruce, The use of magnetic nanoparticles in the development of new molecular detection systems, J. Nanosc. Nanotech. 6 (2006) 1–10.
[38] R. Dalpozzo, Magnetic nanoparticle supports for asymmetric catalysts, Green Chem. 17 (2015) 3671–3686.
[39] O. Marinică, D. Susan-Resiga, F. Bălănean, D. Vizman, V. Socoliuc, L. Vékás, Nano-microcomposite magnetic fluids: magnetic and magnetorheological evaluation for rotating seal and vibration damper applications, J. Magn. Magn. Mater. 406 (2016) 134–143.
[40] C.A. Ross, Patterned magnetic recording media, Annu. Rev. Mater. Sci. 31 (2001) 203–235.
[41] Z. Sun, J. Du, L. Yan, S. Chen, Z. Yang, C. Jing, Multifunctional Fe_3O_4@SiO_2 − Au satellite structured SERS probe for charge selective detection of food dyes, ACS Appl. Mater. Interfaces 8 (2016) 3056–3062.
[42] W.R. Viali, G.B. Alcantara, P.P.C. Sartoratto, M.A.G. Soler, E. Mosiniewicz-Szablewska, B. Andrzejewski, P.C. Morais, Investigation of the molecular surface coating on the stability of insulating magnetic oils, J. Phys. Chem. C 114 (2010) 179–188.
[43] V.M. Aroutiounian, V.M. Arakelyan, G.E. Shahnazaryan, M.S. Aleksanyan, K. Hernadi, Z. Nemeth, P. Berki, Z. Papa, Z. Toth, L. Forro, The ethanol sensors made from α-Fe_2O_3 decorated with multiwall carbon nanotubes, Adv. Nano Res. 3 (2015) 1–11.
[44] Y.P. Chen, M. Zou, C. Qi, M.X. Xie, D.N. Wang, Y.F. Wang, Q. Xue, J.F. Li, Y. Chen, Immunosensor based on magnetic relaxation switch and biotin-streptavidin system for the detection of kanamycin in milk, Biosens. Bioelectron. 39 (2013) 112–117.
[45] A. Zarrin, S. Sadighian, K. Rostamizadeh, O. Firuzi, M. Hamidi, S. Mohammadi-Samani, R. Miri, Design, preparation, and in vitro characterization of a trimodally-targeted nanomagnetic onco-theranostic system for cancer diagnosis and therapy, Int. J. Pharm. 500 (2016) 62–76.
[46] A.E. Deatsch, B.A. Evans, Heating efficiency in magnetic nanoparticle hyperthermia, J. Magn. Magn. Mater. 354 (2014) 163–172.
[47] A.A. Tregubov, I.L. Sokolov, A.V. Babenyshev, P.I. Nikitin, V.R. Cherkasov, M.P. Nikitin, Magnetic hybrid magnetite/metal organic framework nanoparticles: facile preparation, post-synthetic biofunctionalization and tracking in vivo with magnetic methods, J. Magn. Magn. Mater. 449 (2018) 590–596.
[48] W. Aadinath, T. Ghosh, C. Anandharamakrishnan, Multimodal magnetic nano-carriers for cancer treatment: challenges and advancements, J. Magn. Magn. Mater. 401 (1) (2016) 1159–1172.
[49] P.D. Shima, J. Philip, B. Raj, Magnetically controllable nanofluid with tunable thermal conductivity and viscosity, Appl. Phys. Lett. 95 (2009) 133112.
[50] J. Philip, O. Mondain-Monval, F.L. Calderon, J. Bibette, Colloidal force measurements in the presence of a polyelectrolyte, J. Phys. D Appl. Phys. 30 (1997) 2798–2803.
[51] V. Mahendran, J. Philip, Non-enzymatic glucose detection using magnetic nanoemulsions, Appl. Phys. Lett. 105 (2014) 123110.
[52] A.W. Zaibudeen, J. Philip, Magnetic nanofluid based non-enzymatic sensor for urea detection, Sens. Actuators, B 255 (2018) 720–728.
[53] A.W. Zaibudeen, J. Philip, Thermally tunable grating using thermo-responsive magnetic fluid, Opt. Mater. 66 (2017) 117–121.
[54] M.A. Correa-Duarte, M. Giersig, N.A. Kotov, L.M. Liz-Marzán, Control of packing order of self-assembled monolayers of magnetite nanoparticles with and without SiO_2 coating by microwave irradiation, Langmuir 14 (1998) 6430–6435.
[55] F.G. Aliev, M.A. Correa-Duarte, A. Mamedov, J.W. Ostrander, M. Giersig, M. Liz-Marzán, N.A. Kotov, Layer-by-layer assembly of core-shell magnetite nanoparticles: effect of silica coating on interparticle interactions and magnetic properties, Adv. Mater. 11 (1999) 1006–1010.
[56] A.A. Mamedov, N.A. Kotov, Free-standing layer-by-layer assembled films of magnetite nanoparticles, Langmuir 16 (2000) 5530–5533.
[57] A.A. Mamedov, J. Ostrander, F. Aliev, N.A. Kotov, Stratified assemblies of magnetite nanoparticles and montmorillonite prepared by the layer-by-layer assembly, Langmuir 16 (2000) 3941–3949.
[58] H.S. Kim, B.H. Sohn, W. Lee, J.K. Lee, S.J. Choi, S.J. Kwon, Multifunctional layer-by-layer self-assembly of conducting polymers and magnetic nanoparticles, Thin Solid Films 419 (2002) 173–177.
[59] M. Suda, Y. Miyazaki, Y. Hagiwara, O. Sato, S. Shiratori, Y. Einaga, Photoswitchable magnetic layer-by-layer films consisting of azobenzene derivatives and iron oxide nanoparticles, Chem. Lett. 34 (2005) 1028–1029.
[60] D. Grigoriev, D. Gorin, G.B. Sukhorukov, A. Yashchenok, E. Maltseva, H. Möhwald, Langmuir 23 (2007) 12388.
[61] L.G. Paterno, F.J. Fonseca, G.B. Alcantara, M.A.G. Soler, P.C. Morais, J.P. Sinnecker, M.A. Novak, E.C.D. Lima, F.L. Leite, L.H.C. Mattoso, Fabrication and characterization of nanostructured conducting polymer films containing magnetic nanoparticles, Thin Solid Films 517 (2009) 1753.
[62] L.G. Paterno, M.A.G. Soler, F.J. Fonseca, J.P. Sinnecker, E.H.C.P. Sinnecker, E.C.D. Lima, M.A. Novak, P.C. Morais, Layer-by-layer assembly of bifunctional nanofilms: surface-functionalized maghemite hosted in polyaniline, J. Phys. Chem. C 113 (2009) 5087–5095.
[63] A.M. Yashchenok, D.A. Gorin, M. Badylevich, A.A. Serdobintsev, M. Bedard, Y.G. Fedorenko, G.B. Khomutov, D.O. Grigoriev, H. Möhwald, Impact of magnetite nanoparticle incorporation on optical and electrical properties of nanocomposite LbL assemblies, PCCP 12 (2010) 10469–10475.
[64] L.G. Paterno, M.A.G. Soler, J.P. Sinnecker, E.H.C.P. Sinnecker, S.N. Bao, E.C.D. Lima, M.A. Novak, P.C. Morais, Magnetic Nanocomposites fabricated via layer by layer approach, J. Nanosci. Nanotech. 10 (2010) 2679–2685.
[65] S. Dey, K. Mohanta, A.J. Pal, Magnetic-field-assisted layer-by-layer electrostatic assembly of ferromagnetic nanoparticles, Langmuir 26 (2010) 9627–9631.
[66] G.B. Alcantara, L.G. Paterno, A.S. Afonso, R.C. Faria, M.A. Pereira-da-Silva, P.C. Morais, M.A.G. Soler, Adsorption of cobalt ferrite nanoparticle within layer-by-layer films: a kinetic study carried out by quartz crystal microbalance, PCCP 13 (2011) 21233–21242.
[67] G.B. Alcantara, L.G. Paterno, F.J. Fonseca, P.C. Morais, M.A.G. Soler, Morphology of cobalt ferrite nanoparticle-polyelectrolyte multilayered nanocomposites, J. Magn. Magn. Mater. 323 (2011) 1372–1377.
[68] B.P. Pichon, P. Louet, O. Felix, M. Drillon, S. Begin-Colin, G. Decher, Magnetotunable hybrid films of stratified iron oxide nanoparticles assembled by the layer-by-layer technique, Chem. Mater. 23 (2011) 3668–3675.
[69] L.G. Paterno, E.H.C.P. Sinnecker, M.A.G. Soler, J.P. Sinnecker, M.A. Novak, P.C. Morais, Tuning of magnetic dipolar interactions of maghemite nanoparticles embedded in polyelectrolyte layer-by-layer films, J. Nanosci. Nanotechnol. 12 (2012) 6672–6678.
[70] M.A.G. Soler, L.G. Paterno, J.P. Sinnecker, J.G. Wen, E.H.C.P. Sinnecker, R.F. Neumann, M. Bahiana, M.A. Novak, P.C. Morais, Assembly of c-Fe_2O_3/polyaniline nanofilms with tuned dipolar interaction, J. Nanoparticle Res. 14 (2012) 653–710.
[71] I. Dincer, O. Tozkoparan, S.V. German, A.V. Markin, O. Yildirim, G.B. Khomutov, D.A. Gorin, S.B. Venig, Y. Elerman, Effect of the number of iron oxide nanoparticle layers on the magnetic properties of nanocomposite LbL assemblies, J. Magn. Magn. Mater. 324 (2012) 2958–2963.
[72] R.F. Neumann, M. Bahiana, L.G. Paterno, M.A.G. Soler, J.P. Sinnecker, J.G. Wen, P.C. Morais, Morphology and magnetism of multifunctional nanostructured γ-Fe_2O_3 films: simulation and experiments, J. Magn. Magn. Mater. 347 (2013) 26–32.
[73] D. Choi, B. Son, T.H. Park, J. Hong, Controlled surface functionality of magnetic nanoparticles by layer-by-layer assembled nano-films, Nanoscale 7 (2015) 6703–6711.
[74] W. Shi, R. Liang, S. Xu, Y. Wang, C. Luo, M. Darwish, S.K. Smoukov, Layer-by-layer self-assembly: toward magnetic films with tunable anisotropy, J. Phys. Chem. C 119 (2015) 13215–13223.
[75] C.J. Letti, L.G. Paterno, M.A. Pereira-da-Silva, P.C. Morais, M.A.G. Soler, The role of polymer films on the oxidation of magnetite nanoparticles, Solid State Chem. 246 (2017) 57–64.
[76] C.J. Letti, K.A.G. Costa, M.A. Gross, L.G. Paterno, M.A. Pereira-da-Silva, P.C. Morais, M.A.G. Soler, Synthesis, morphology and electrochemical applications of iron oxide based nanocomposites, Adv. Nano Res. 5 (3) (2017) 215–230.
[77] J.B. Schlenoff, H. Ly, M. Li, Charge and mass balance in polyelectrolyte multilayers, J. Am. Chem. Soc. 120 (1998) 7626–7634.
[78] S. Krupicka, P. Novák, Oxide spinels, ferromagnetic materials, North-Holland Publishing Company, Amsterdan, 1982 Vol III.
[79] G.A. Ferguson Jr., M; Hass, Magnetic structure and vacancy distribution in γ-Fe_2O_3 by neutron diffraction, Phys. Rev. 112 (1958) 1130–1131.
[80] H.T. Jeng, G.Y. Guo, First-principles investigations of the electronic structure and magnetocrystalline anisotropy in strained magnetite Fe_3O_4, Phys. Rev. B 65 (2002) 094429.
[81] M. Opel, Spintronic oxides grown by laser-MBE, J. Phys. D Appl. Phys. 45 (2012) 033001.
[82] L. Néel, Théorie du trainage magnétique des ferrogamgnétiques en grains fins avec applications aux terres cuites, Ann. Geophys. 5 (1949) 99.
[83] M.A.G. Soler, E.C.D. Lima, S.W. da Silva, T.F.O. Melo, A.C.M. Pimenta, J.P. Sinnecker, R.B. Azevedo, V.K. Garg, A.C. Oliveira, M.A. Novak, P.C. Morais, Aging investigation of cobalt ferrite nanoparticles in low pH magnetic fluid, Langmuir 23 (2007) 9611–9617.
[84] J. Park, J. Joo, S.G. Kwon, Y. Jang, T. Hyeon, Synthesis of monodisperse spherical nanocrystals, Angew. Chem. Int. Ed. 46 (2007) 4630–4660.

[85] E. Blums, A. Cebers, M.M. Maiorov, Magnetic Fluids, Walter de Gruyter, Berlin, 1985.
[86] S. Begin-Colin, D. Felder-Flesch, Functionalizsation of magnetic iron oxide nanoparticles, in: N.T.K. Thank (Ed.), Magnetic Nanoparticles from Fabrication to Clinical Applications, CRC Press Taylor & Francis Group, Boca Raton, FL, 2012, pp. 151–191.
[87] T. Kang, F. Li, S. Baik, W. Shao, D. Ling, T. Hyeon, Surface design of magnetic nanoparticles for stimuli-responsive cancer imaging and therapy, Biomaterials 136 (2017) 98–114.
[88] L. Trahms, Biomedical applications of magnetic nanoparticles, in: S. Odenbach (Ed.), Colloidal Mangetic Fluids, Verlag, Berlim Weidelberg, 2010, pp. 328–358.
[89] S.A. Chambers, Epitaxial growth and properties of doped transition metal end complex oxide films, Adv. Mater. 22 (2010) 219–247.
[90] F.V. de Sales, S.W. Silva, J.M.R. Cruz, A.F.G. do Monte, M.A.G. Soler, P.C. Morais, M.J. da Silva, A.A. Quivy, Indications of amplified spontaneous emission in the energy transfer between InAs self-assembled quantum dots, Phys. Rev. B 70 (2004) 235318.
[91] A. Izquierdo, S.S. Ono, J.C. Voegel, P. Schaaf, G. Decher, Dipping versus spraying: exploring the deposition conditions for speeding up layer-by-layer assembly, Langmuir 21 (21) (2005) 7558–7567.
[92] J.J. Richardson, M. Björnmalm, F. Caruso, Technology-driven layer-by-layer assembly of nanofilms, Science 348 (2015) 2491.
[93] J.T. O'Neal, M.J. Bolen, E.Y. Dai, J.L. Lutkenhaus, Hydrogen-bonded polymer nanocomposites containing discrete layers of gold nanoparticles, J. Colloid Interface Sci. 485 (2017) 260–268.
[94] G. Sauerbrey, Z. Physik, Verwendung von Schwingquarzen zur Wäigung dünner Schichten und zur Mikrowäigung, 155 (1959) 206 – 222.
[95] R.F.M. Lobo, M.A. Pereira-da-Silva, M. Raposo, R.M. Faria, O.N. Oliveira Jr., In situ thickness measurements of ultra-thin multilayer polymer films by atomic force microscopy, Nanotechnology 10 (1999) 389–393.
[96] S.W. Silva, T. Melo, M.A.G. Soler, M.F. Da Silva, E.C.D. Lima, P.C. Morais, Stability of citrate-coated magnetite and cobalt-ferrite nanoparticles under laser irradiation: a Raman spectroscopy investigation, IEEE Trans. Magn. 39 (2003) 2645–2647.
[97] M.A.G. Soler, Q. Fanyao, Raman spectroscopy of iron oxide nanoparticles, Raman Spectroscopy for Nanomaterials Characterization, Springer-Verlag, Berlin, 2012, pp. 379–417.
[98] G.S. Braga, L.G. Paterno, J.P.H. Lima, F.J. Fonseca, A.M. de Andrade, Influence of the deposition parameters on the morphology and electrical conductivity of PANI/PSS self-assembled films, Mater. Sci. Eng., C 28 (2008) 555–562.
[99] A. Rebolledo, A. Fuertes, T. Gonzalez-Carreño, M. Sevilla, T. Valdes-Solis, P. Tartaj, Signatures of clustering in superparamagnetic colloidal nanocomposites of an inorganic and hybrid nature, Small 4 (2) (2008) 254–261.
[100] M. Buján-Núñez, N. Fontaiña-Troitiño, C. Vázquez-Vázquez, M. López- Quintela, Y. Piñeiro, D. Serantes, D. Baldomir, J. Rivas, Influence of the nanoparticle size on the blocking temperature of interacting systems: Monte Carlo simulations, J. Non-Cryst. Solids 354 (47–51) (2008) 5222–5223.
[101] F. Hoppe, M. Arturo Rivadulla, M. Carmen Lopez-Quintela, J. Bujan, D. Rivas, D. Baldomir Serantes, Effect of submicrometer clustering on the magnetic properties of free-standing superparamagnetic nanocomposites, J. Phys. Chem. C 112 (34) (2008) 13099–13104.
[102] S. Lamba, S. Annapoorni, Single domain magnetic arrays: role of disorder and interactions, Eur. Phys. J. B 39 (1) (2004) 19–25.
[103] L. Machala, R. Zboril, A. Gedanken, Amorphous iron(III) oxides – a review, J. Phys. Chem. B 111 (2007) 4003–4018.
[104] R.W. Chantrell, N.S. Walmsley, J. Gore, M. Maylin, Initial susceptibility of interacting fine particles, J. Magn. Magn. Mater. 196–197 (1999) 118–119.
[105] D. Fiorani, A.M. Testa, F. Lucari, F. D'Orazio, H. Romero, Physica B 320 (2002) 122–126.
[106] J.L. Dormann, L. Spinu, E. Tronc, J.P. Jolivet, F. Lucari, F. D'Orazio, D. Fiorani, Effect of interparticle interactions on the dynamical properties of γ -Fe_2O_3 nanoparticles, J. Magn. Magn. Mater. 183 (1998) L255–L260.
[107] J.L. Dormann, D. Fiorani, E. Tronc, Magnetic relaxation in fine-particle systems, in: I. Prigogine, S.A. Rice (Eds.), Adv. Chem. Phys. 98 1997, pp. 283–494.
[108] J.I. Gittleman, B. Abeles, S. Bozowski, Superparamagnetism and relaxation effects in granular Ni-SiO_2 and Ni-Al_2O_3 films, Phys. Rev. B 9 (1974) 3891–3897.
[109] M.A. Novak, W.S.D. Folly, J.P. Sinnecker, S. Sorian, Relaxation in magnetic nanostructures, J. Magn. Magn. Mater. 294 (2005) 133–140.
[110] M. Bahiana, Y. Oono, Cell dynamical system approach to block copolymers, Phys. Rev. A 41 (1990) 6763–6771.
[111] U. Nowak, R.W. Chantrell, E.C. Kennedy, Monte Carlo simulation with time step quantification in terms of Langevin dynamics, Phys. Rev. Lett. 84 (2000) 163–166.
[112] J.P. Pereira Nunes, M. Bahiana, C.S.M. Bastos, Magnetization curves as probes of Monte Carlo simulation of nonequilibrium states, Phys. Rev. E 69 (2004) 56703.
[113] E. Barsoukov, J.R. Macdonald, Impedance Spectroscopy: Theory, Experiment and Applications, VCH, New Jersey, 2005.